

# Invariant computations in local cortical networks with balanced excitation and inhibition

Jorge Mariño<sup>1,3</sup>, James Schummers<sup>1</sup>, David C Lyon<sup>1,3</sup>, Lars Schwabe<sup>2</sup>, Oliver Beck<sup>2</sup>, Peter Wiesing<sup>2</sup>, Klaus Obermayer<sup>2</sup> & Mriganka Sur<sup>1</sup>

Cortical computations critically involve local neuronal circuits. The computations are often invariant across a cortical area yet are carried out by networks that can vary widely within an area according to its functional architecture. Here we demonstrate a mechanism by which orientation selectivity is computed invariantly in cat primary visual cortex across an orientation preference map that provides a wide diversity of local circuits. Visually evoked excitatory and inhibitory synaptic conductances are balanced exquisitely in cortical neurons and thus keep the spike response sharply tuned at all map locations. This functional balance derives from spatially isotropic local connectivity of both excitatory and inhibitory cells. Modeling results demonstrate that such covariation is a signature of recurrent rather than purely feed-forward processing and that the observed isotropic local circuit is sufficient to generate invariant spike tuning.

Processing networks in sensory cortex carry out transformations on their inputs so as to create outputs that are relevant for perception and action. These transformations are characteristic of an area, rely on discrete local circuits and are computed both dynamically and invariantly despite variations in functional architecture within the area<sup>1</sup>. For example, the computation of feature-selective responses, such as orientation selectivity in primary visual cortex (V1), involves the integration of excitatory and inhibitory inputs arising from a variety of sources to produce responses that are sharply tuned for the orientation of visual stimuli and that are also influenced adaptively by the history of stimulation<sup>2–6</sup>. An understanding of these computations requires a description of the behavior of neurons within the context of their cortical circuit<sup>2,7,8</sup>. The composition of the local circuit varies systematically across the orientation preference map in V1 (refs. 9,10); the local network near pinwheel centers contains a broad orientation distribution, whereas the network far from pinwheels, in orientation domains, contains a homogeneous representation. The impact of a neuron's local neighborhood on its responses has recently been described in V1 of cats: neurons at pinwheel centers have more broadly tuned subthreshold responses compared with neurons in orientation domains<sup>11,12</sup>, yet the spike responses are sharply tuned for orientation whatever the orientation map location<sup>13,14</sup>. Recent studies *in vitro* and *in vivo* have emphasized the interplay between excitation and inhibition as an essential mechanism for stabilizing and shaping neural activity<sup>15–17</sup>. Here we have examined the mechanism by which invariant orientation tuning is created in V1 despite the diversity of local environments, by measuring electrophysiologically the excitatory and inhibitory synaptic conductances in neurons at different map

positions and describing anatomically the inputs to these neurons. Computational models of cellular and network behavior support the conclusion that the cortical network operates in a recurrent rather than a purely feed-forward mode, and that simple rules of spatial integration of excitation and inhibition can explain sharp orientation tuning at all locations in the orientation map.

## RESULTS

### Synaptic conductances at different map locations

We combined optical imaging of intrinsic signals and whole-cell recordings *in vivo* (see Methods and **Supplementary Figs. 1 and 2** online) to measure the orientation tuning of synaptic conductances of cells located at different sites in the orientation preference map of cat V1. Illustrated here are data from two cells, one located in an orientation domain (**Fig. 1a–d**) and another at a pinwheel center (**Fig. 1e–h**). The spike responses of both cells were sharply tuned for orientation (**Fig. 1b,f**). The visually evoked membrane potential response ( $V_m$ ), obtained with different levels of intracellular current injection (**Fig. 1d,h**), was used to calculate changes in total conductance ( $g$ )<sup>18,19</sup>. For 7/7 orientation domain cells and 7/11 pinwheel cells, the preferred orientation of  $g$  was aligned (within  $\pm 22.5^\circ$ ) with the preferred orientation of the spiking response. The remaining four pinwheel neurons showed a displacement of 45–67.5° in the peak  $g$  relative to spike tuning. This difference was due to broadly tuned conductances rather than to a rotation of narrow  $g$  tuning curves. The degree of selectivity was quantified using the orientation selectivity index (OSI), which is a global measure of tuning across the entire tuning curve<sup>11</sup>. Orientation domain cells displayed a clear difference in the magnitude of  $g$  between

<sup>1</sup>Department of Brain and Cognitive Sciences and Picower Center for Learning and Memory, Massachusetts Institute of Technology, Cambridge, Massachusetts 02139, USA.

<sup>2</sup>Department of Computer Science and Electrical Engineering, Berlin University of Technology, FR2-1, Franklinstrasse 28/29, 10587, Berlin, Germany. <sup>3</sup>Present addresses: Department of Medicine, Neuroscience and Motor Control Group (Neurocom), Univ. A Coruña, Fac. CC. da Saúde, Campus de Oza, 15006, A Coruña, Spain (J.M.), The Salk Institute, SNL-C, 10010 North Torrey Pines Road, La Jolla, California 92037, USA (D.C.L.). Correspondence should be addressed to M.S. (msur@mit.edu).

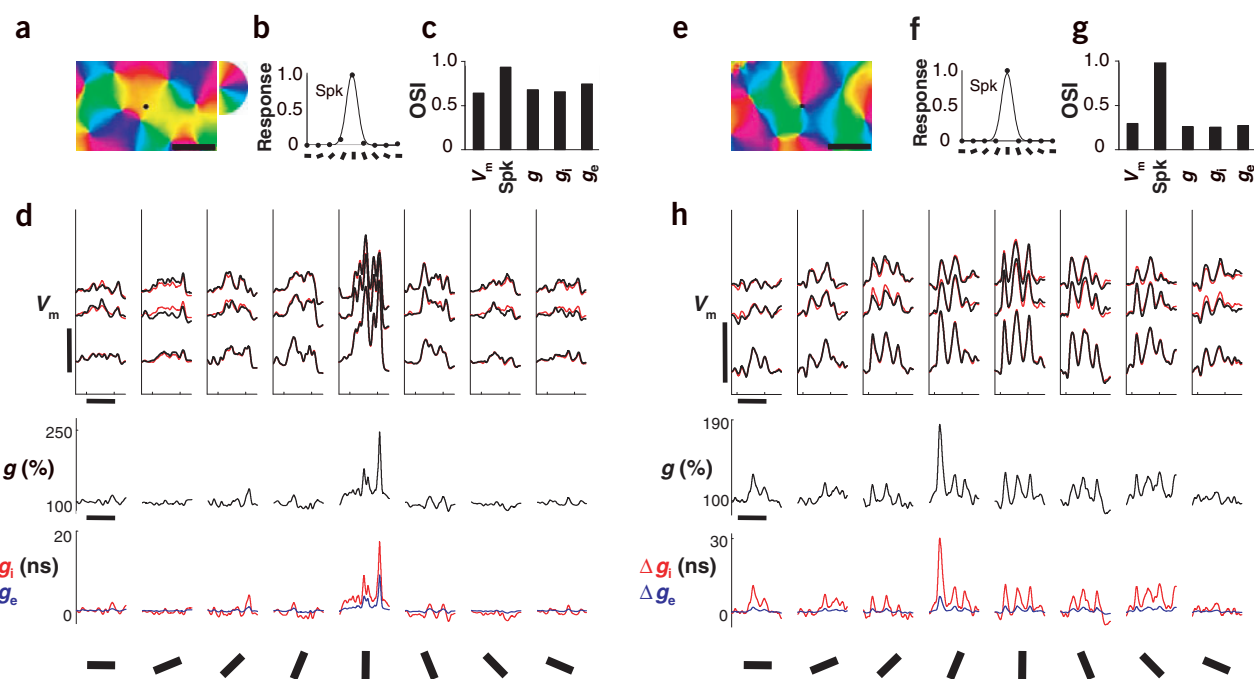


**Figure 1** Orientation tuning of synaptic conductances for a cell in an orientation domain (**a–d**) and at a pinwheel center (**e–h**). (**a,e**) Orientation preference maps from V1 (a small region is shown, from a large region that was imaged). Filled circles indicate the location of recording electrodes. Color-coded semicircle in **a** indicates the angle of orientation preference of each pixel. Scale bars: 500  $\mu\text{m}$ . (**b,f**) Orientation tuning curves of the spike responses. (**c,g**) OSIs calculated for the membrane potential ( $V_m$ ), spike response (Spk), total conductance ( $g$ ) and inhibitory and excitatory conductances ( $g_i$  and  $g_e$ ).  $V_m$  and the underlying conductances ( $g$ ,  $g_i$  and  $g_e$ ) are relatively narrowly tuned for the orientation domain cell but are broadly tuned for the pinwheel center cell. Spike tuning is invariably sharp for both cells. (**d,h**) Traces of the average visually evoked changes in  $V_m$ ,  $g$ ,  $g_i$  and  $g_e$  in response to each of eight stimulus orientations spanning 180°. (Top rows)  $V_m$  traces. Black lines show the mean activity for three to five trials under resting conditions and for two levels of current injection (–0.2 and 0.1 nA). Red lines show the predicted  $V_m$  traces from linear regression fits used to obtain  $g$  (see Methods). The predicted and actual traces are in good agreement. Horizontal scale under  $g$ , 1 s (visual stimulation time); vertical scale, 10 mV in **d** and 5 mV in **h**. (Middle rows)  $g$  traces showing changes relative to rest. (Bottom rows)  $\Delta g_i$  and  $\Delta g_e$  traces showing absolute changes in  $g_i$  and  $g_e$ .

preferred and orthogonal stimulation (leading to high OSI values; **Fig. 1c**), whereas for pinwheel neurons there was a large increase in  $g$  for all stimulus orientations (leading to low OSI values; **Fig. 1g**).

To reveal the synaptic mechanisms involved in the transformation of the diverse  $g$  tuning curves at different map locations into uniformly sharp spike tuning, we calculated the visually evoked changes in inhibitory and excitatory conductances ( $g_i$  and  $g_e$ )<sup>4,19</sup>. The mean absolute change in inhibitory conductance was always larger than for excitation, independent of orientation or map location. Similar to the differences observed for  $g$ , the OSIs for  $g_i$  and  $g_e$  were lower for pinwheel cells (**Fig. 1c,g**). **Figure 2** shows, for four additional cells, the relationship between the OSI of visually evoked increases in  $g_i$  and  $g_e$  and map location. Orientation domain cells (**Fig. 2a,b**) responded to their preferred orientation with a large increase in  $g_i$  and  $g_e$  when compared with the orthogonal orientation, but this difference was smaller for pinwheel cells (**Fig. 2c,d**), giving rise to lower OSIs. For all cells, the OSI values for  $g_i$  and  $g_e$  covaried, indicating that regardless of location, inhibition always seemed to balance excitation. Laminal position and receptive field type<sup>20,21</sup> (simple or complex) may also influence the integration of inputs by V1 cells. We conducted a three-way ANOVA to compare OSIs for  $g$ ,  $g_i$  and  $g_e$  between map locations (pinwheel/domain), recording depth and cell type, and found a significant effect of orientation map location (all  $P$  values < 0.007) but no effect of the other two variables (all  $P$  values > 0.3). Subsequently, for the population analysis (**Fig. 3**), we did not differentiate between cell types or cortical depths.

Compared with orientation domains, the average tuning curve for  $g_e$  in pinwheels was broader and showed a larger offset at orthogonal orientations (**Fig. 3b**). This could potentially be explained by an isotropic pattern of local connections, in which neurons located at or near pinwheel centers would receive inputs from neurons with different orientation preferences, flattening the  $V_m$  and conductance tuning curves (**Fig. 3a**), whereas orientation domain cells would be primarily driven by cells sharing the same orientation. **Figure 3b** shows that increases in  $g_i$  run in parallel with  $g_e$ ; this inhibition, probably a mechanism to counteract the excitatory input, is especially prominent in pinwheel neurons at nonpreferred orientations, allowing these cells to display a sharp spike tuning despite broad excitatory inputs. The population analysis indicated that OSIs for both  $g_i$  and  $g_e$  (**Fig. 3c**) are significantly different between neurons located in orientation domains and pinwheel centers ( $P < 0.002$  for  $g_i$ ,  $P < 0.001$  for  $g_e$ ), indicating that V1 neurons receive different inputs depending on their location in the orientation map. The source of this heterogeneity is probably the structure of the map itself. Because we directed our recordings to orientation domains and pinwheel centers, these differences probably show the two extremes of a more gradual variation along the orientation map. To quantify the specificity of the surrounding orientation representation, we calculated the OSI of the orientation distribution of pixel counts in the map surrounding each neuron; cells located at pinwheels have low local input OSIs, whereas the OSIs are progressively higher as neurons move toward a domain center<sup>11,14</sup>. We found a significant correlation ( $r = 0.79$ ,  $P < 0.0001$ ) between the OSI of the conductance tuning curve and

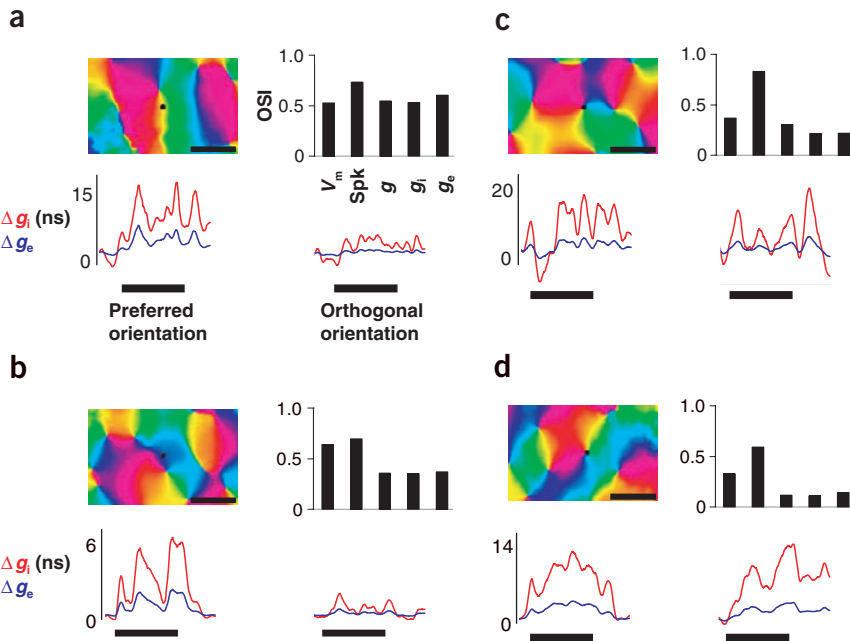


**Figure 2** Additional examples of conductance tuning of cells in orientation domains and pinwheel centers. (**a,b**) Two examples of changes in  $g_i$  and  $g_e$  following visual stimulation (1 s, bars below traces) in orientation domain cells, and the associated OSIs for  $V_m$ , spike activity and changes in conductance. All conventions are as in **Figure 1**. (**c,d**) Two examples of conductance changes and OSIs in pinwheel cells. All conventions are as in **Figure 1**.

a domain and a pinwheel injection is depicted (**Fig. 4b**). Independent of location, the pattern of labeled cells around the injection site was always roughly circular, ignoring the distribution of orientation preferences<sup>24</sup>. This distribution of cells, as shown for the two individual cases (**Fig. 4c**) and for the population (**Fig. 4d**), indicated a local isotropic radius of influence of  $\sim 250 \mu\text{m}$ . We computed orientation tuning curves of the inputs to each injection site by assigning an orientation preference to each labeled cell according to the optically imaged orientation preference map recorded in the same animal. Within this radius, the OSIs

the OSI of the local input region (**Fig. 3d**), suggesting a relationship between the tuning of synaptic inputs and the orientation representation in the local circuit across a cortical distance of only a few hundred microns. A similar relationship exists for  $g_i$  and  $g_e$  (see **Fig. 5g,h**), and indeed between  $g_i$  and  $g_e$  ( $r = 0.99$ ,  $P < 0.0001$ ). These relationships support the proposal that observed variations in the tuning of  $g$ ,  $g_i$  and  $g_e$  are related to functional heterogeneities in the local inputs. The data suggest the existence of a single mechanism that is able to balance the different patterns of excitation and inhibition at different locations, keeping the spike response equally selective at any site. Thus, we proposed that the different tuning curves of conductance at different locations of the orientation map may be achieved by a common principle: a spatially isotropic pattern of local excitatory and inhibitory connections. The heterogeneity in tuning of synaptic inputs would then be a consequence of applying a uniform rule of anatomical pooling and synaptic integration to a heterogeneous functional map. To explore this possibility, we first examined the anatomical distribution of local excitatory and inhibitory inputs to neurons at different locations in the orientation map and subsequently used single-neuron and network models to analyze the effect of synaptic pooling within the anatomical input zone on  $g$ ,  $V_m$  and spike responses.

### Anatomical inputs to different map locations

We used extremely small injections (uptake zone  $< 100 \mu\text{m}$  in diameter) of retrograde tracers to study the structure of local inputs to different sites in the orientation map, combined with labeling for GABAergic cells (**Fig. 4a**). Distributions of inhibitory neurons have been described less completely in previous reports<sup>22,23</sup>. Our technique of double-labeling cells from very small tracer injection and staining for the GABA antibody allowed us to demonstrate for the first time a more complete view of the distribution of local excitatory and inhibitory cells in V1. More importantly, our technique provided a fine-grained comparison of the projection patterns to orientation domains and pinwheel centers. Despite drastic differences in local orientation distributions at pinwheels and domains, we found no differences in the spatial distribution of either local inhibitory or excitatory cells labeled at these sites (**Fig. 4b–d**). An example of the pattern of retrogradely labeled cells from

for cells labeled by pinwheel injections ( $n = 3$ ) were much lower than those for orientation domains ( $n = 4$ ) (**Fig. 4e**). **Figure 4e** also shows that the OSI differences between pinwheels and domains were similar for inhibitory and excitatory cells. Thus, the anatomical data provide a potential substrate for the electrophysiological measurements, suggesting that broader excitatory and inhibitory synaptic conductances at pinwheel centers arise naturally from spatially isotropic local projections.

### Model tuning at different map locations

The pattern of anatomical connections can be combined with the strength of synaptic drive to explain the physiological responses of neurons. We used complementary single-neuron and network models to derive the excitatory and inhibitory conductances under which spike tuning of V1 neurons would be invariant with map location, which we then compared with the measured conductances. Thus, we first set up a Hodgkin-Huxley type single-neuron model<sup>25</sup> (see Methods and **Supplementary Notes** online for a detailed description). By convolving the experimentally obtained spatial excitatory input profiles (**Fig. 4d**) with experimentally obtained orientation maps, we calculated the tuning of the excitatory conductance  $g_e$  at locations ranging from pinwheels to domains. Then, given these  $g_e$  curves, we determined the  $g_i$  tuning curves that yield sharp spike tuning for each location (**Fig. 5a,b**, and **Supplementary Fig. 3a** online). These tuning curves are similar to the experimentally measured  $g_e$  and  $g_i$  tuning curves (**Fig. 3b**). Furthermore, the offset and slope for the OSIs as a function of local input OSIs fall within the 95% confidence interval of the experimentally measured values (see **Supplementary Fig. 3a** online). As with the experimental data, the difference between pinwheel locations and orientation domains is reflected in the subthreshold signal, but as a result of the appropriate inhibitory balance at orthogonal orientations, which keeps the membrane potential below threshold, it is not reflected in the spike responses (**Fig. 5c,d** and **Supplementary Fig. 3** online). These model results indicate that, given the constraints of anatomical location within an orientation map, the inhibitory tuning that we measured resembles the tuning that is necessary, in theory, to balance excitation and yield sharp spike tuning at all locations.

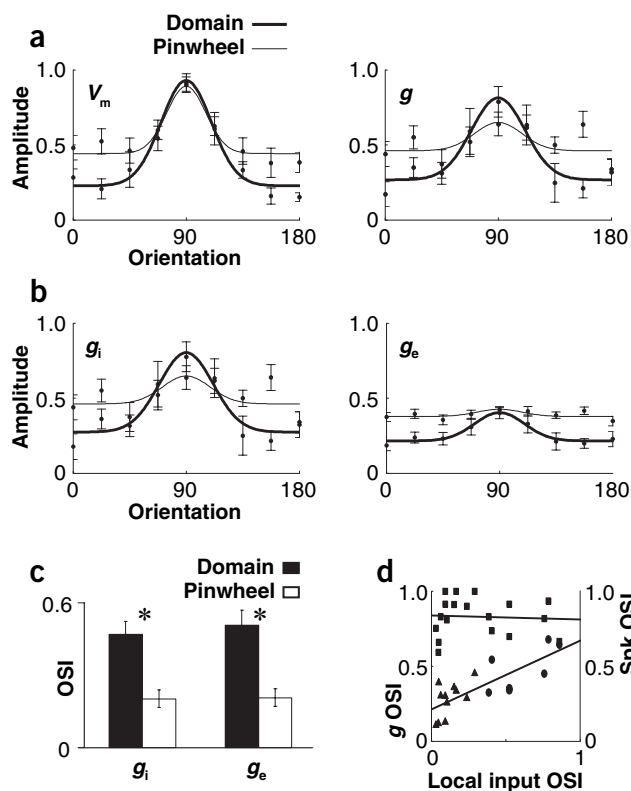


**Figure 3** Average tuning differences between cells at pinwheels and orientation domains. **(a)** Normalized tuning curves for mean changes in  $V_m$  and  $g$  in orientation domain and pinwheel neurons ( $\pm$  s.e.m.). A Gaussian function is fitted to the data for illustration purposes only; all quantitative comparisons are based on OSIs derived from actual data points for each cell. **(b)** Normalized tuning curves for changes in  $g_i$  and  $g_e$  in orientation domain and pinwheel cells. Both conductances were normalized together for each individual cell, and then population means were computed. Conventions are as in **a**. **(c)** Bar plot comparing mean  $g_i$  and  $g_e$  OSIs for the population of orientation domain and pinwheel cells. Asterisks: Student's *t*-test,  $P < 0.002$ . **(d)** Scatter plot of the OSI values of  $g$  and the OSIs of the local input region (radius: 250  $\mu$ m) for each recorded neuron. The orientation distribution of pixels in this local region was calculated from the actual orientation preference map. Triangles: pinwheel cells; circles: domain cells. Lower line is the least-squares linear fit to the data ( $r = 0.79$ ;  $P < 0.0001$ ). For comparison, the OSI values (squares) and linear fit (upper line;  $r = -0.06$ ;  $P = 0.82$ ) of the spike response (Spk) are also shown.

(the signature of a recurrent versus a feed-forward mode) no longer fell within the 95% confidence interval from the measurements. These simulations demonstrate that the tuning curves of the excitatory and inhibitory conductances deduced with the single-cell model indeed occur in a recurrent network, if the local excitatory and inhibitory synaptic inputs are balanced and both contribute significantly to the driving input.

## DISCUSSION

Our results show that visual stimulation evokes a different pattern of synaptic inputs at orientation domains compared with pinwheel centers. We demonstrate that these response patterns result from diverse synaptic inputs impinging on different locations in the orientation map, acting through a locally isotropic and recurrent anatomical architecture. That is, the spatial distribution of excitatory and inhibitory neurons provides the necessary anatomical inputs, and their synaptic drive provides sufficient functional balance to preserve sharp spike tuning, particularly at pinwheel centers.

### The role of inhibition in orientation selectivity

The generation of orientation selectivity in visual cortex includes mechanisms that shape two related aspects of a neuron's response: its preferred orientation and its orientation selectivity or tuning strength. Recent evidence suggests that the preferred orientation of a V1 neuron arises from the feed-forward bias of its afferent inputs<sup>29–31</sup>. Orientation selectivity seems to be narrower than afferent spread and probably requires intracortical mechanisms for its generation<sup>12</sup>. These mechanisms potentially include the spike threshold of the neuron, recurrent excitation between cortical neurons and intracortical inhibition. The spike threshold is a nonlinearity that sharpens the selectivity of spike outputs relative to the selectivity of excitatory synaptic inputs<sup>32,33</sup>. It has been suggested that the spike threshold is dynamically regulated to enhance orientation selectivity<sup>34</sup>, but there is no evidence that the spike threshold varies with map location. The role of intracortical excitation and inhibition in generating orientation selectivity remains unresolved<sup>2,3,35,36</sup>. If intracortical mechanisms were to have a role, it is probable that their effect would be observed most clearly at pinwheels, where the local cortical network would provide broadly tuned excitation, and inhibition would be required to counter this spread. Our experimental results are consistent with recent findings that broad subthreshold excitation is present at pinwheels<sup>11,12</sup>, and we now demonstrate that inhibition balances excitation so that both are required for sharp spike tuning.

These results help reconcile several findings that seem to contradict each other, particularly in relation to the preferred orientation and tuning

Finally, we examined whether the necessary covariation between excitation and inhibition also emerges in a cortical network similar to V1. In a previous modeling study of a V1 network that explicitly included pinwheels and orientation domains<sup>26,27</sup>, it was concluded that local isotropic connectivity leads to orientation tuning of spike responses that strongly depend on location in the orientation map, and in particular to sharper tuning at pinwheel centers (a prediction not supported by experimental findings<sup>11,13,14</sup>, including the present study) (Figs. 1,2). Thus, we set up a large-scale network of Hodgkin-Huxley type model neurons to determine whether and under what conditions it can produce the covarying excitation and inhibition leading to sharp orientation tuning invariant with map location. In the absence of evidence for location-specific feed-forward tuning, we assumed that the afferent drive is tuned similarly for cells across the map. Unlike previous models<sup>7,8,28</sup>, the model network had identical local excitatory and inhibitory connection length scales, determined from the results of our tracer injection experiments (Fig. 4d; see Supplementary Notes online) and was parameterized first to operate in a regime in which the recurrent excitation contributes considerably to visual responses. The model's predicted tuning for  $g_i$  and  $g_e$  is shown in Figure 5e for pinwheels and orientation domains. Figure 5f–h shows that the tuning of  $g$ ,  $g_i$  and  $g_e$  clearly depended on the local input OSI and hence on map location, matching the covarying excitatory and inhibitory conductance OSIs measured experimentally. The slope and intercept values for this relationship fell within the 95% confidence intervals from the measured values. As in the single-cell model, this led to location-independent spike tuning (see Supplementary Fig. 4 online). We then parameterized our model to operate in a range of conditions, including a regime in which recurrent excitation was weak, inhibition dominated and the neurons were mainly driven by feed-forward inputs. In this case, excitation and inhibition did not covary, and the spike tuning became dependent on map location (see Supplementary Fig. 5 online). Now the slope of  $g_e$

of inhibition and its contribution to orientation selectivity. Measurements of the excitatory and inhibitory synaptic conductances underlying orientation tuning in cat V1 have found large conductance changes<sup>18</sup> but either strictly iso-oriented inhibition<sup>19</sup> or diversity in the preferred orientation of inhibition<sup>4</sup>. We show that the diversity can be explained at least in part by map location: orientation domains contain iso-oriented excitation and inhibition, whereas pinwheels can show variable relationships among excitation, inhibition and spike tuning, owing mainly to broadly tuned conductances rather than to narrowly tuned cross-oriented inhibition. Other reasons for divergent preferred orientations may include differences in the stimulus (full-field gratings versus bars) or uncontrolled differences in laminar position<sup>21</sup>. Measurements of the time course of responses in monkey V1 have found either stable tuning<sup>37,38</sup> or dynamic changes in tuning over time, including strong suppression of nonpreferred orientations late in the response<sup>39</sup>. Our findings predict that response dynamics would be more variable at pinwheels than at orientation domains (and would be seen in a relatively small proportion of randomly sampled cells, because regions of rapid orientation change such as pinwheels and their neighborhood occupy a small fraction of the cortical surface<sup>14</sup>). Indeed, reverse correlation analyses at pinwheels and orientation domains in cat V1 support this prediction (J. Schummers, J. Mariño, M. Sur, *Soc. Neurosci. Abstr.* 818.6, 2003).

Pharmacological manipulation of inhibitory inputs to neurons have also shown either no effect of intracellular inhibitory blockade on

orientation selectivity<sup>40</sup> or a broadening of tuning following extracellular iontophoresis of blockers at cross-oriented sites ~500  $\mu\text{m}$  away<sup>36</sup>. A plausible explanation for the former result is that intracellular blockade of inhibition at orientation domains may have little effect on tuning. For the latter result, the effect would be much greater at pinwheels, where nearby sites also probably have very different preferred orientations. Overall, it is probable that the tuning of neurons near pinwheel centers is more sensitive to changes in the balance of inhibition and excitation. This proposal is supported by the finding that visual pattern adaptation induces short-term shifts in the preferred orientation and tuning strength of neurons much more readily at pinwheels than at orientation domains<sup>14</sup>.

#### Invariant tuning with balanced excitation and inhibition

Consistent with a previous report<sup>19</sup>, we demonstrate a close relationship between the spread of excitation and inhibition, which are similarly tuned regardless of map location. The source of these synaptic inputs is probably the local neighborhood of a neuron<sup>24</sup>, although we cannot rule out at least excitatory inputs from iso-oriented sites that are located more distantly<sup>41,42</sup>. Importantly, although previous models of orientation selectivity have invoked broader inhibition compared with excitation<sup>7,8,28</sup> to generate sharp tuning, our single-cell and network models show that balanced excitation and inhibition are sufficient to produce sharp tuning at all locations. Furthermore, in contrast to recent models that are based on an idealized structure of orientation maps<sup>26,27</sup>, our network model has the distinct advantage of incorporating parameters based on experimentally measured spatial profiles of excitatory and inhibitory convergence and projecting these spatial profiles onto experimentally obtained orientation maps. Future work will need to address the possible influence of the

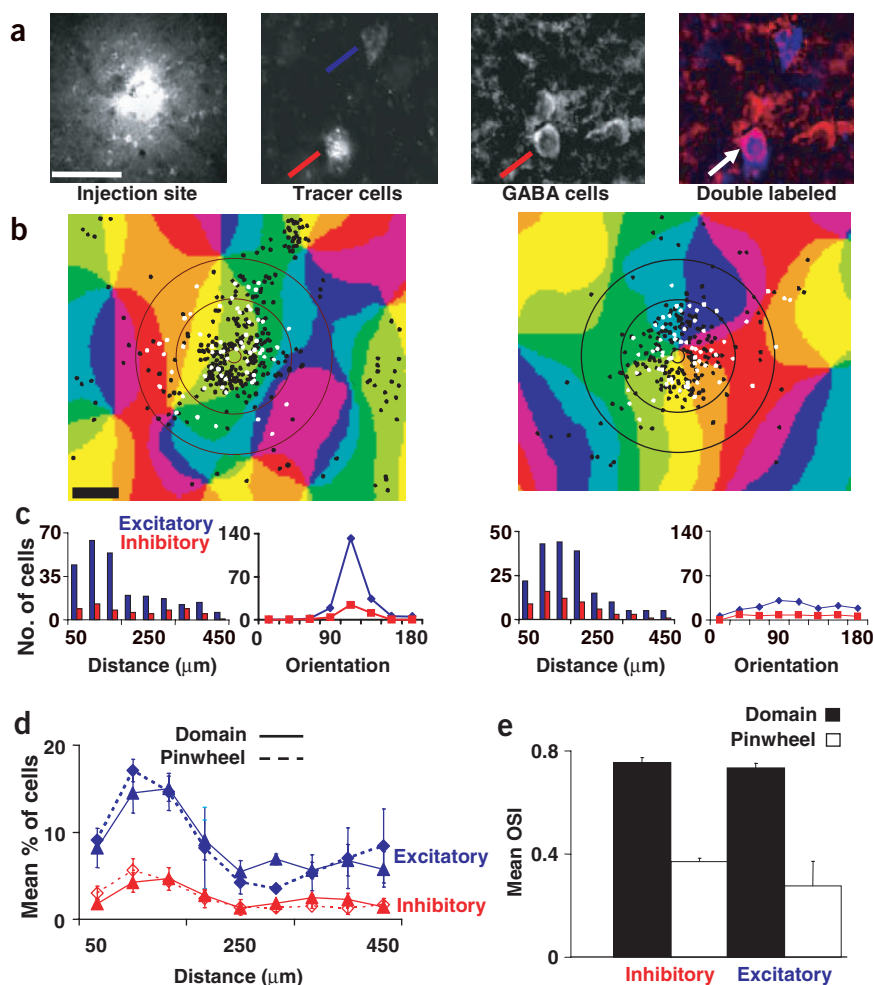


**Figure 4** Anatomical analysis of local excitatory and inhibitory projections to pinwheel centers and orientation domains. **(a)** Example of an injection site (scale bar: 100  $\mu\text{m}$ ), and three images of the same region showing retrogradely labeled, GABA-positive and double-labeled cells, respectively. For illustration purposes, the two middle images were high-pass filtered and merged to show the double-labeled neurons at right. **(b)** Examples of the distribution of cells within the orientation map following an injection of tracer in an orientation domain (left) and a pinwheel center (right). Black: excitatory cells; white: inhibitory cells. The two outer concentric circles are at 250- $\mu\text{m}$  intervals from the injection site (inner circle). Scale bar: 250  $\mu\text{m}$ . **(c)** Histograms and tuning curves computed from the orientation domain (left) and pinwheel (right) cells depicted in **b**. Histograms show the number of inhibitory and excitatory cells located at different distances from the injection. The orientation tuning curves indicate the number of inhibitory and excitatory cells found in the different orientation regions, within a distance of 250  $\mu\text{m}$ . **(d)** Population curves of three pinwheel and four domain injections showing the proportion of inhibitory and excitatory cells found at different distances from the injection. **(e)** Bar plot of the mean OSIs for the population data. Error bars in **d** and **e** show s.e.m.

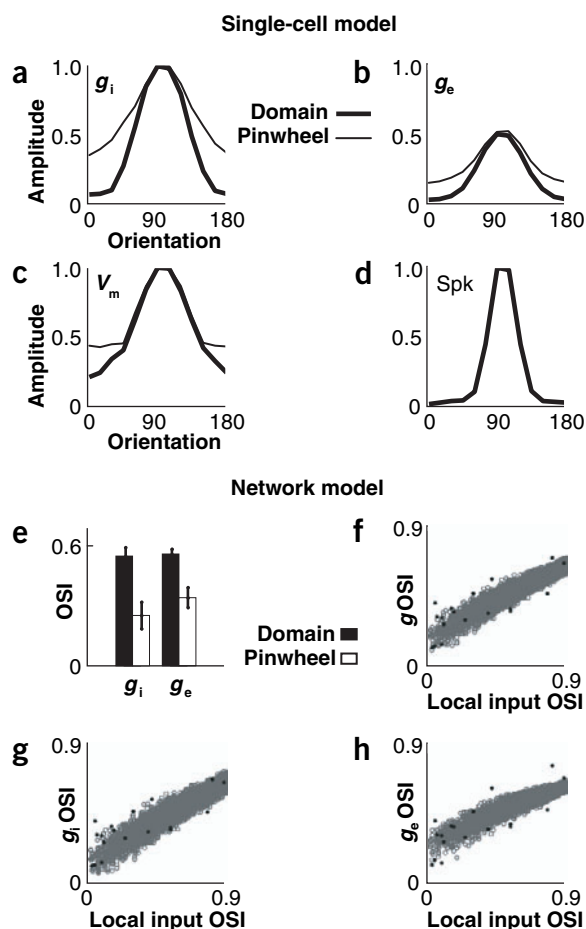


**Figure 5** Model predictions for synaptic conductances, membrane potentials and spike responses underlying orientation selectivity across the orientation map. (a,b) Inhibitory and excitatory conductance tuning for a pinwheel cell and an orientation domain cell derived from the single-cell model. The afferent input in orientation space is described by a Gaussian function,  $\sigma = 25^\circ$ , added to an offset of 10% of the maximum value. (c)  $V_m$  tuning at a pinwheel center and in an orientation domain with the input conductances from a and b. (d) Spike response tuning at a pinwheel center and in an orientation domain (the two are nearly identical but have different  $V_m$  tuning as shown in c, created by different  $g_i$  and  $g_e$  tuning as shown in a and b). (e) OSIs of  $g_i$  and  $g_e$  for pinwheels and orientation domains derived from the network model. (f) OSIs of the total conductance as a function of the local input OSI for the network model (gray), and data points from the experiments (black). (g,h) OSIs of  $g_i$  and  $g_e$  as a function of the local input OSI for the network model (gray), and data points from the experiments (black).

Although the match between the tuning of conductance and of the local orientation network is comparable in our data and model, there is more scatter in the data. This may result from small errors in localization of electrode penetrations (**Supplementary Fig. 2** online), pooling of data from different cortical layers, or other experimental variables. Another possible source of noise in the data is the influence of dendritic processing. We have measured synaptic conductances at the soma, but inputs to the dendrites may well be different from what is detectable at the soma<sup>44</sup>.

In addition to location invariance, the orientation selectivity of V1 responses is also invariant with stimulus contrast, in which intracortical inhibition has a crucial role<sup>7,45</sup>. Recent simulations<sup>46</sup> and experimental<sup>47</sup> work have proposed the existence in cortical layer 4 of two functionally different types of inhibition, generated by simple cells with sharp orientation tuning and by untuned complex cells, respectively. The balance of excitation and inhibition described here is related to the functional architecture of the orientation preference map, without regard to laminar location or cell type. It is still unknown if the proposed difference between inhibitory neurons holds for other cortical layers and, if so, what might be the relative contribution of each type to their target cell responses. Our results are compatible with the presence of both types of cells: simple inhibitory cells would provide the observed tuned responses, whereas an orientation-independent offset could be regulated by inhibition from complex cells.

In sum, the measurements of synaptic conductances and anatomical inputs, together with the models of single cells and local networks, provide a comprehensive description of the integration of inputs that underlies the computation of orientation tuning in V1. We have found that a simple rule of spatial integration ensures a balance of excitation and inhibition that produces sharp orientation tuning at all positions in the orientation map. A homeostatic balance between excitation and inhibition has been proposed as a mechanism for the regulation of synaptic strength in developing networks<sup>15,48</sup> and for the consolidation of functional connections in cortex during a critical period of visual development<sup>49,50</sup>. Our results demonstrate, for the first time, the fundamental role of such a balance for a key emergent computation in the adult visual cortex. A similar mechanism based on the balance provided by local inputs may account for the tuning of other functional properties in visual cortex, and may be a general mechanism for generating and preserving response selectivity in sensory cortex<sup>16,17</sup>.

## METHODS

**Animals.** Experiments were done on 23 adult cats that were anesthetized and paralyzed. Stabilization for physiological recordings was achieved through stereotaxic fixation of the head, suspension at lumbar level, drainage of cerebrospinal fluid

temporal structure of voltage fluctuations<sup>34,43</sup> and the relative timing of excitation and inhibition<sup>16</sup>.

Our conductance measurements, together with our network model, constrain the regime in which visual cortex networks probably operate to generate orientation tuning. We show that a purely feed-forward regime is incompatible with the data: the regime predicts that the tuning of  $g_e$  would show no relationship to map location, whereas the data show a strong relationship between the tuning of  $g_e$  and the local orientation distribution. (Because the tuning of  $g_i$  derives mainly from the local inhibitory network, it is always location dependent, being broad at pinwheels and narrow at orientation domains. A feed-forward model would thus generate sharper spike tuning at pinwheels than at orientation domains, which is not seen experimentally.) The model operates in a balanced regime in which recurrent excitation contributes significantly to neuronal responses, but not in an extreme recurrent regime, or 'marginal phase'<sup>28</sup>, where the afferent input 'selects' predefined response patterns and the tuning width is strongly determined by the pattern of orientation-selective intracortical connections. In the model's regime, predetermined response patterns do not exist; rather, the tuning depends on characteristics of the afferent input. Hence, broadly tuned afferent input does not lead to sharp output tuning as expected for a network operating in the marginal phase, but moderately tuned afferent input is sharpened by the cortical network (**Supplementary Notes**). Furthermore, in this regime, the tuning of  $g_e$  correlates well with map location, matches the measured data closely, is balanced by a covarying  $g_i$ , and generates location-independent spike tuning.

and bilateral pneumothorax. Subsequent to performance of a craniotomy and durotomy over V1, a steel chamber was mounted on the skull and filled with agar (2% in saline). Eyes were protected with contact lenses and focused on a computer monitor using appropriate lenses. EEG, EKG, expired CO<sub>2</sub> and rectal temperature were continuously monitored and used to assess the state of the animal. All protocols were approved by MIT's Animal Care and Use Committee and conformed to US National Institutes of Health (NIH) guidelines.

**Optical imaging.** Techniques for intrinsic-signal optical imaging were similar to those we have described elsewhere<sup>9,11</sup>. Responses to full-field drifting square-wave gratings of eight orientations were used to compute orientation preference (angle) maps. Special care was taken in choosing highly accurate and reproducible maps. First, reference images of the surface vasculature were obtained after every 20 trials (~100 min). Only maps in which there was zero movement were deemed acceptable. Second, angle maps were computed from independent blocks of 15–20 trials and compared. Third, angle maps were computed from the two independent sets of four orientations contained within the stimulus set. If shifts in pinwheel center location or other systematic discrepancies in the layout of the map were observed, recordings were discontinued until the preparation was stabilized. Imaging was only terminated after the independent maps showed extremely minor differences. Furthermore, the specific sites to be targeted for patch recordings or tracer injection were chosen to be the most stable sites, assessed as just described. In most cases, we were able to find pinwheel centers that shifted by no more than 1–2 pixels (13–26 μm). An analysis of the reliability of pinwheel center localization is described in **Supplementary Notes** online (see also **Supplementary Fig. 2** online).

**Electrophysiology.** Procedures for *in vivo* whole-cell recording were similar to those used previously by us<sup>11,40</sup> and others<sup>4,19,47</sup>. Glass microelectrodes (resistance 6–12 MΩ) filled with a patch solution<sup>4,11</sup> were carefully lowered into the cortex and directed to either orientation domains or pinwheel centers, using an image of the surface vasculature aligned to the orientation map as reference. Recordings were made in bridge mode; the extracellularly measured electrode resistance ( $R_e$ ) was neutralized at the beginning of each penetration. Visual stimuli were randomly generated drifting sine-wave gratings of eight orientations, moving in opposite directions, plus a blank stimulus, each of which was presented five times for 1 s. This protocol was repeated while injecting three to four different steady currents ( $I_{inj}$ ) ranging from –0.2 to 0.1 nA. Cell parameters were monitored every stimulus cycle by means of I–V curves. The entire protocol was completed in 40 cells, from which 18 were chosen for further analysis according to their stable biophysical properties. The average series resistance was  $70.5 \pm 39.7$  MΩ (mean  $\pm$  s.d.), input resistance  $27.8 \pm 20.1$  MΩ, time constant  $17.4 \pm 8$  ms and resting potential  $-50.4 \pm 15.1$  mV. Compensation for series resistance, input conductance measurements and reliability of the measurements were made using quantitative methods similar to those described by others<sup>16,19</sup>. Briefly,  $R_e$  was calculated offline by fitting a double exponential to the cell's response to current pulses (I–V curves), and its contribution to the membrane potential ( $V_m$ ) was subtracted from the traces. Total conductance  $g(t)$  at time  $t$  was estimated by regression as the inverse of the slope of a line fitted to the relation between  $I_{inj}$  and  $V_m$ . To calculate the inhibitory  $g_i(t)$  and excitatory  $g_e(t)$  conductances, we assumed  $g(t) = g_e(t) + g_i(t)$ , and

$$V_{rest}(t) = [g_e(t)E_e + g_i(t)E_i]/[g_e(t) + g_i(t)]$$

where  $V_{rest}(t)$  is the membrane potential in the absence of current injection, and  $E_e$  and  $E_i$  are the equilibrium potentials for  $g_e(t)$  and  $g_i(t)$ , respectively. Then,  $g_i(t)$  and  $g_e(t)$  can be derived as follows:

$$g_i(t) = [g(t)(V_{rest}(t) - E_e)]/E_i - E_e$$

$$g_e(t) = [g(t)(V_{rest}(t) - E_i)]/E_e - E_i$$

We used  $E_e = 0$  mV and  $E_i = -80$  mV (for the latter, we analyzed all cells using different values between –70 and –90 mV; these had no substantial effects on the main results). The  $g(t)$  values obtained from linear regression fits were used

to predict the  $V_m$  values at each time point; these were compared to the actual values as a goodness-of-fit measure (**Fig. 1**).

For each cell, we calculated the orientation tuning curve and OSI for spiking activity,  $V_m$ ,  $g$ ,  $g_i$  and  $g_e$ . The OSI is the magnitude of the vector average of the responses to all stimulus orientations, computed as

$$OSI = [\sqrt{(\sum R(\theta_i) \cos(2\theta_i))^2 + (\sum R(\theta_i) \sin(2\theta_i))^2}]/[\sum R_i]$$

where  $R$  is average response during grating presentation and  $\theta$  is orientation from 0 to 157.5, indexed by  $i = 1$  to 8. It is a continuous measure with values ranging from 0 (unselective) to 1 (perfectly selective).

**Anatomy.** In V1 of nine cats, glass pipettes (tip diameter 10–20 μm) were used to place three distinct injections (25 nL; pressure injected with a Pico Spritzer II; General Valve) of fluorescent conjugates of cholera toxin subunit B (CTB) (2%; Alexa-Fluor 488, 594 and 647; Molecular Probes) in pinwheels and domains at a depth of ~600 μm. After 36–48 h, the cats were given an overdose of sodium pentobarbital, perfused, and their brains processed. V1 was removed and sectioned (40 μm) tangential to the surface. The tissue was processed to reveal GABA<sup>+</sup> neurons by using a GABA antibody (1:500, rabbit; Sigma) and Alexa-Fluor 350 goat anti-rabbit IgG (1:200).

Images of the pattern of labeled neurons near the depth of the injection and laterally were acquired with a Zeiss Axiocam system. Inhibitory neurons were identified by positive staining for the GABA antibody and double labeling from tracer injection. The pattern of labeled cells was aligned to the orientation map using landmarks from three injection sites, visible penetrations from the patch pipettes and blood vessel patterns along the cortical surface and through a depth of 600 μm.

To ensure the most detailed anatomical analysis of local connectivity from our sample of 27 injections, we limited analysis to three pinwheel and four domain injections, selected because their spread of tracer uptake was confined to a diameter <100 μm. For these injections, the numbers of excitatory and inhibitory neurons were counted every 50 μm from the boundary of the injection site to a radius of 450 μm.

**Computer simulations.** The single-neuron model used (one compartment, Hodgkin-Huxley type neuron, with Na<sup>+</sup>, K<sup>+</sup> and M currents and balanced background noise inputs<sup>25</sup>) is described in detail in **Supplementary Notes** online. Briefly, presynaptic activity (independent Poisson spike trains) was separated into background, feed-forward and recurrent components, which describe the continuing activity not dependent on the stimulus, the afferent stimulus-driven input and the inputs due to the activation of the local network neighborhood. Probabilities of intracortical synaptic connections with presynaptic excitatory neurons were estimated from optically imaged orientation maps. The total excitatory input conductance, given as a function of stimulus orientation, was then computed for local neighborhoods of varying OSI under the assumption that the spike tuning of all excitatory neurons is the same and independent of location in the orientation map. Then the tuning curve of the total inhibitory conductance necessary to obtain the observed sharp tuning curve of the firing rates was calculated.

The large-scale network model is also described in detail in **Supplementary Notes** online. Its main features were as follows: first, the model was composed of Hodgkin-Huxley type point neurons similar to that used for the single-cell model, received synaptic background activity, and had synaptic currents modeled as originating from GABA, AMPA and NMDA receptors. Second, experimentally obtained optically imaged orientation maps were used for assigning orientation preferences to cortical locations. In addition, artificial orientation maps were used for comparison with other models<sup>26</sup>. The network was composed of up to  $128 \times 128$  neurons and modeled a patch of cortex  $2.25 \times 2.25$  mm<sup>2</sup> in size. Third, the afferent inputs to cortical cells were broadly tuned ( $\sigma = 27.5^\circ$ ) and were described by Poisson spike trains with a time-independent firing rate. Fourth, spatially isotropic synaptic connections in cortical space, with experimentally determined radial profiles ( $r = 250$  μm) for excitation and inhibition, were used. Fifth, we explored a range of parameters, importantly varying the relative strength of the afferent and the recurrent inputs.

*Note: Supplementary information is available on the Nature Neuroscience website.*

## ACKNOWLEDGMENTS

This work was supported by Ministerio de Educación y Ciencia, Spain (J.M.), Howard Hughes Medical Institute (J.S.), Deutsche Forschungsgemeinschaft Sonderforschungsbereiche 618, Germany (L.S., O.B., K.O.), Wellcome Trust (P.W., K.O.) and National Institutes of Health (D.C.L., M.S.).

## COMPETING INTERESTS STATEMENT

The authors declare that they have no competing financial interests.

Received 12 November 2004; accepted 21 December 2004

Published online at <http://www.nature.com/natureneuroscience/>

1. Mountcastle, V.B. *Perceptual Neuroscience* (Harvard University Press, Cambridge, MA, 1998).
2. Ferster, D. & Miller, K.D. Neural mechanisms of orientation selectivity in the visual cortex. *Annu. Rev. Neurosci.* **23**, 441–471 (2000).
3. Martin, K.A. Microcircuits in visual cortex. *Curr. Opin. Neurobiol.* **12**, 418–425 (2002).
4. Monier, C., Chavane, F., Baudot, P., Graham, L.J. & Fregnac, Y. Orientation and direction selectivity of synaptic inputs in visual cortical neurons: a diversity of combinations produces spike tuning. *Neuron* **37**, 663–680 (2003).
5. Yao, H. & Dan, Y. Stimulus timing-dependent plasticity in cortical processing of orientation. *Neuron* **32**, 315–323 (2001).
6. Dragoi, V. & Sur, M. Plasticity of orientation processing in adult visual cortex. in *The Visual Neurosciences* (eds. Chalupa, L.M. & Werner, J.S.) 1654–1664 (MIT Press, Cambridge, Massachusetts, 2003).
7. Somers, D.C., Nelson, S.B. & Sur, M. An emergent model of orientation selectivity in cat visual cortical simple cells. *J. Neurosci.* **15**, 5448–5465 (1995).
8. Suarez, H., Koch, C. & Douglas, R. Modeling direction selectivity of simple cells in striate visual cortex within the framework of the canonical microcircuit. *J. Neurosci.* **15**, 6700–6719 (1995).
9. Bonhoeffer, T. & Grinvald, A. Iso-orientation domains in cat visual cortex are arranged in pinwheel-like patterns. *Nature* **353**, 429–431 (1991).
10. Das, A. & Gilbert, C.D. Topography of contextual modulations mediated by short-range interactions in primary visual cortex. *Nature* **399**, 655–661 (1999).
11. Schummers, J., Mariño, J. & Sur, M. Synaptic integration by V1 neurons depends on location within the orientation map. *Neuron* **36**, 969–978 (2002).
12. Sharon, D. & Grinvald, A. Dynamics and constancy in cortical spatiotemporal patterns of orientation processing. *Science* **295**, 512–515 (2002).
13. Maldonado, P.E., Godecke, I., Gray, C.M. & Bonhoeffer, T. Orientation selectivity in pinwheel centers in cat striate cortex. *Science* **276**, 1551–1555 (1997).
14. Dragoi, V., Rivadulla, C. & Sur, M. Foci of orientation plasticity in visual cortex. *Nature* **411**, 80–86 (2001).
15. Turrigiano, G.G. & Nelson, S.B. Homeostatic plasticity in the developing nervous system. *Nat. Rev. Neurosci.* **5**, 97–107 (2004).
16. Wehr, M. & Zador, A.M. Balanced inhibition underlies tuning and sharpens spike timing in auditory cortex. *Nature* **426**, 442–446 (2003).
17. Zhang, L.I., Tan, A.Y., Schreiner, C.E. & Merzenich, M.M. Topography and synaptic shaping of direction selectivity in primary auditory cortex. *Nature* **424**, 201–205 (2003).
18. Borg-Graham, L.J., Monier, C. & Fregnac, Y. Visual input evokes transient and strong shunting inhibition in visual cortical neurons. *Nature* **393**, 369–373 (1998).
19. Anderson, J.S., Carandini, M. & Ferster, D. Orientation tuning of input conductance, excitation, and inhibition in cat primary visual cortex. *J. Neurophysiol.* **84**, 909–926 (2000).
20. Hirsch, J.A. *et al.* Synaptic physiology of the flow of information in the cat's visual cortex *in vivo*. *J. Physiol.* **540**, 335–350 (2002).
21. Martinez, L.M., Alonso, J.M., Reid, R.C. & Hirsch, J.A. Laminar processing of stimulus orientation in cat visual cortex. *J. Physiol.* **540**, 321–333 (2002).
22. Kisvarday, Z.F., Toth, E., Rausch, M. & Eysel, U.T. Orientation-specific relationship between populations of excitatory and inhibitory lateral connections in the visual cortex of the cat. *Cereb. Cortex* **7**, 605–618 (1997).
23. Roerig, B. & Chen, B. Relationships of local inhibitory and excitatory circuits to orientation preference maps in ferret visual cortex. *Cereb. Cortex* **12**, 187–198 (2002).
24. Yousef, T., Toth, E., Rausch, M., Eysel, U.T. & Kisvarday, Z.F. Topography of orientation centre connections in the primary visual cortex of the cat. *Neuroreport* **12**, 1693–1699 (2001).
25. Destexhe, A., Rudolph, M., Fellous, J.M. & Sejnowski, T.J. Fluctuating synaptic conductances recreate *in vivo*-like activity in neocortical neurons. *Neuroscience* **107**, 13–24 (2001).
26. McLaughlin, D., Shapley, R., Shelley, M. & Wieland, D.J. A neuronal network model of macaque primary visual cortex (V1): orientation selectivity and dynamics in the input layer 4C. *Proc. Natl. Acad. Sci. USA* **97**, 87–92 (2000).
27. Wieland, D.J., Shelley, M., McLaughlin, D. & Shapley, R. How simple cells are made in a nonlinear network model of the visual cortex. *J. Neurosci.* **21**, 5203–5211 (2001).
28. Ben-Yishai, R., Bar-Or, R.L. & Sompolinsky, H. Theory of orientation tuning in visual cortex. *Proc. Natl. Acad. Sci. USA* **92**, 3844–3848 (1995).
29. Mooser, F., Bosking, W.H. & Fitzpatrick, D. A morphological basis for orientation tuning in primary visual cortex. *Nat. Neurosci.* **7**, 872–879 (2004).
30. Reid, R.C. & Alonso, J.M. Specificity of monosynaptic connections from thalamus to visual cortex. *Nature* **378**, 281–284 (1995).
31. Lampl, I., Anderson, J.S., Gillespie, D.C. & Ferster, D. Prediction of orientation selectivity from receptive field architecture in simple cells of cat visual cortex. *Neuron* **30**, 263–274 (2001).
32. Carandini, M. & Ferster, D. Membrane potential and firing rate in cat primary visual cortex. *J. Neurosci.* **20**, 470–484 (2000).
33. Volgushev, M., Pernberg, J. & Eysel, U.T. Comparison of the selectivity of postsynaptic potentials and spike responses in cat visual cortex. *Eur. J. Neurosci.* **12**, 257–263 (2000).
34. Azouz, R. & Gray, C.M. Adaptive coincidence detection and dynamic gain control in visual cortical neurons *in vivo*. *Neuron* **37**, 513–523 (2003).
35. Shapley, R., Hawken, M. & Ringach, D.L. Dynamics of orientation selectivity in the primary visual cortex and the importance of cortical inhibition. *Neuron* **38**, 689–699 (2003).
36. Crook, J.M., Kisvarday, Z.F. & Eysel, U.T. GABA-induced inactivation of functionally characterized sites in cat striate cortex: effects on orientation tuning and direction selectivity. *Vis. Neurosci.* **14**, 141–158 (1997).
37. Mazer, J.A., Vinje, W.E., McDermott, J., Schiller, P.H. & Gallant, J.L. Spatial frequency and orientation tuning dynamics in area V1. *Proc. Natl. Acad. Sci. USA* **99**, 1645–1650 (2002).
38. Dragoi, V., Sharma, J., Miller, E.K. & Sur, M. Dynamics of neuronal sensitivity in visual cortex and local feature discrimination. *Nat. Neurosci.* **5**, 883–891 (2002).
39. Ringach, D.L., Bredfeldt, C.E., Shapley, R.M. & Hawken, M.J. Suppression of neural responses to nonoptimal stimuli correlates with tuning selectivity in macaque V1. *J. Neurophysiol.* **87**, 1018–1027 (2002).
40. Nelson, S., Toth, L., Sheth, B. & Sur, M. Orientation selectivity of cortical neurons during intracellular blockade of inhibition. *Science* **265**, 774–777 (1994).
41. Bosking, W.H., Zhang, Y., Schofield, B. & Fitzpatrick, D. Orientation selectivity and the arrangement of horizontal connections in tree shrew striate cortex. *J. Neurosci.* **17**, 2112–2127 (1997).
42. Angelucci, A. *et al.* Circuits for local and global signal integration in primary visual cortex. *J. Neurosci.* **22**, 8633–8646 (2002).
43. Volgushev, M., Pernberg, J. & Eysel, U.T.  $\gamma$ -Frequency fluctuations of the membrane potential and response selectivity in visual cortical neurons. *Eur. J. Neurosci.* **17**, 1768–1776 (2003).
44. Williams, S.R. Spatial compartmentalization and functional impact of conductance in pyramidal neurons. *Nat. Neurosci.* **7**, 961–967 (2004).
45. Troyer, T.W., Krukowski, A.E., Priebe, N.J. & Miller, K.D. Contrast-invariant orientation tuning in cat visual cortex: thalamocortical input tuning and correlation-based intracortical connectivity. *J. Neurosci.* **18**, 5908–5927 (1998).
46. Lauritzen, T.Z. & Miller, K.D. Different roles for simple-cell and complex-cell inhibition in V1. *J. Neurosci.* **23**, 10201–10213 (2003).
47. Hirsch, J.A. *et al.* Functionally distinct inhibitory neurons at the first stage of visual cortical processing. *Nat. Neurosci.* **6**, 1300–1308 (2003).
48. Liu, G. Local structural balance and functional interaction of excitatory and inhibitory synapses in hippocampal dendrites. *Nat. Neurosci.* **7**, 373–379 (2004).
49. Desai, N.S., Cudmore, R.H., Nelson, S.B. & Turrigiano, G.G. Critical periods for experience-dependent synaptic scaling in visual cortex. *Nat. Neurosci.* **5**, 783–789 (2002).
50. Fagiolini, M. & Hensch, T.K. Excitatory-inhibitory balance controls critical period plasticity. in *Excitatory-Inhibitory Balance: Synapses, Circuits, Systems* (eds. Hensch, T.K. & Fagiolini, M.) 269–282 (Kluwer Academic/Plenum, New York, 2003)